Journal of *Marine Science and Engineering*

MDPI

*Article*

# Physical Implementation and Experimental Validation of the Compensation Mechanism for a Ramp-Based AUV Recovery System

**Zhaoji Qi [1,2], Lingshuai Meng [1,*], Haitao Gu [1], Ziyang Guo [1,3], Jinyan Wu [1,2] and Chenghui Li [1,2]**

[1] State Key Laboratory of Robotics, Shenyang Institute of Automation, Chinese Academy of Sciences, Shenyang 110016, China; qizhaoji@sia.cn (Z.Q.); guhaitao@sia.cn (H.G.); guoziyang@sia.cn (Z.G.); wujinyan@sia.cn (J.W.); lichenghui@sia.cn (C.L.)
[2] University of Chinese Academy of Sciences, Beijing 100049, China
[3] School of Mechanical Engineering, Shenyang University of Technology, Shenyang 110870, China
* Correspondence: menglingshuai@sia.cn

**Abstract**

In complex marine environments, ramp-based recovery systems for autonomous underwater vehicles (AUVs) often encounter engineering challenges such as reduced docking accuracy and success rate due to disturbances in the capture window attitude. In this study, a desktop-scale physical experimental platform for recovery compensation was designed and constructed. The system integrates attitude feedback provided by an attitude sensor and dual-motor actuation to achieve active roll and pitch compensation of the capture window. Based on the structural and geometric characteristics of the platform, a dual-channel closed-loop control strategy was proposed utilizing midpoint tracking of the capture window, accompanied by multi-level software limit protection and automatic centering mechanisms. The control algorithm was implemented using a discrete-time PID structure, with gain parameters optimized through experimental tuning under repeatable disturbance conditions. A first-order system approximation was adopted to model the actuator dynamics. Experiments were conducted under various disturbance scenarios and multiple control parameter configurations to evaluate the attitude tracking performance, dynamic response, and repeatability of the system. The results show that, compared to the uncompensated case, the proposed compensation mechanism reduces the *MSE* by up to 76.4% and the *MaxAE* by 73.5%, significantly improving the tracking accuracy and dynamic stability of the recovery window. The study also discusses the platform's limitations and future optimization directions, providing theoretical and engineering references for practical AUV recovery operations.

**Keywords:** AUV recovery; compensation mechanism; desktop experimental platform; attitude control; PID control; engineering validation; autonomous docking

check for updates

Received: 24 June 2025
Revised: 10 July 2025
Accepted: 14 July 2025
Published: 16 July 2025

**Citation:** Qi, Z.; Meng, L.; Gu, H.; Guo, Z.; Wu, J.; Li, C. Physical Implementation and Experimental Validation of the Compensation Mechanism for a Ramp-Based AUV Recovery System. *J. Mar. Sci. Eng.* **2025**, *13*, 1349. https://doi.org/10.3390/jmse13071349

**Copyright:** © 2025 by the authors. Licensee MDPI, Basel, Switzerland. This article is an open access article distributed under the terms and conditions of the Creative Commons Attribution (CC BY) license (https://creativecommons.org/licenses/by/4.0/).

## 1. Introduction

In recent years, the rapid development of both surface and underwater autonomous platforms has significantly promoted the application of intelligent marine systems in fields such as resource exploration, environmental monitoring, infrastructure inspection, and search and rescue operations [1,2]. Among these platforms, autonomous underwater vehicles (AUVs) have become essential equipment for deep-sea operations due to their high autonomy, excellent maneuverability, and strong environmental adaptability, and have been

widely applied in marine scientific research, engineering surveys, and underwater mission execution [2,3]. Meanwhile, unmanned surface vehicles (USVs), as important collaborative platforms for AUV operations and autonomous recovery, are increasingly utilized in coastal inspections, offshore monitoring, and multi-system coordinated tasks [4,5]. However, the deployment and recovery processes of AUVs remain the most hazardous and failure-prone stages throughout the mission cycle. Ensuring the safety and success rate of AUV recovery operations, especially under complex sea conditions, has become a key technical challenge restricting the practical application of intelligent marine equipment [6].

Currently, AUV recovery methods mainly include crane-based recovery, A-frame recovery, ramp-based recovery, and moonpool recovery [3,6]. These traditional recovery methods generally rely on large manned vessels or engineering platforms, which are associated with complex operations, poor adaptability to sea conditions, and significant challenges in system integration [7]. In recent years, with the rapid development of unmanned surface vehicle (USV) technology, autonomous recovery of AUVs based on USV platforms has become an important development trend of intelligent marine systems. Compared with other approaches, ramp-based recovery systems have gradually become the mainstream technical solution for integrating AUV autonomous recovery on USV platforms, owing to their simple structure, strong adaptability to sea conditions, and minimal structural modification requirements for the mother vessel [8,9].

However, in complex sea conditions, the ramp platform and its recovery window are often subjected to multi-degree-of-freedom attitude disturbances caused by waves, swells, and vessel motions, which severely affect the spatial alignment accuracy of the AUV and the recovery window, thereby reducing the overall operational safety and recovery success rate [10]. In response to these challenges, various control strategies and structural optimization methods have been proposed. Some studies have implemented autonomous compensation for the recovery window based on visual guidance, acoustic positioning, and ultra-short baseline (USBL) technology [11,12]. Meanwhile, dynamic recovery methods based on deep reinforcement learning and adaptive control have also become research hotspots in recent years, effectively improving the environmental adaptability and compensation performance of recovery systems to a certain extent [13,14]. However, most existing studies are still limited to theoretical analysis or simulation validation, lacking low-cost, practically replicable physical experimental platforms and systematic dynamic performance testing, which significantly constrain the engineering application of ramp-based AUV autonomous recovery technology.

Despite certain progress in the structural design and control methods of ramp-based AUV autonomous recovery systems, there are still significant limitations in attitude disturbance compensation, spatial alignment accuracy, and dynamic response performance under the high uncertainty of actual sea conditions and the delayed dynamic response characteristics of the platform. Particularly, under multi-degree-of-freedom composite disturbances induced by waves, traditional ramp systems lack efficient real-time attitude sensing and rapid compensation mechanisms, making it difficult to maintain the spatial stability of the recovery window and further reducing the success rate of autonomous recovery operations and the overall reliability of the system [15].

In recent years, some studies have conducted dynamic modeling and motion compensation analysis for ramp-based AUV recovery platforms and proposed dynamic control methods based on the sliding-rail structure [15]. Meanwhile, in order to improve the attitude control accuracy and robustness of AUV autonomous docking systems, researchers have explored two-step control approaches, vision-guided techniques, and intelligent compensation strategies based on reinforcement learning, which have demonstrated certain levels of environmental adaptability and dynamic compensation effectiveness in theoretical

analyses and simulation studies [16,17]. However, most of the existing work remains at the stage of theoretical models or limited laboratory testing, lacking low-cost, compact, and practically replicable physical experimental platforms and systematic dynamic performance evaluations, which restrict the practical application and engineering development of ramp-based AUV autonomous recovery systems.

In addition to these advanced methods, conventional control strategies such as proportional–derivative (PD) and proportional–integral–derivative (PID) controllers are widely applied due to their simple implementation, real-time response, and engineering practicality [18,19]. Meanwhile, previous studies have conducted dynamic modeling and control analysis for low-degree-of-freedom systems, providing theoretical references for motion compensation design [20]. However, PD/PID controllers often face limitations in parameter tuning and robustness when dealing with highly uncertain and dynamic sea conditions. More advanced techniques, such as fuzzy logic control [21], robust control [22], and reinforcement learning-based adaptive strategies, provide enhanced disturbance rejection and environmental adaptability, but typically require complex algorithm design, high computational resources, and extensive system modeling, which restrict their practical application in low-cost, compact recovery platforms.

To address the above-mentioned technical challenges, this study designs and implements a ramp-based AUV recovery compensation experimental platform. The system integrates an attitude sensor, a dual-motor cable-driven actuation mechanism, and a dual-channel closed-loop control system to enable active adjustment of the recovery window. A dynamic compensation strategy based on midpoint tracking is introduced, along with multi-level software limits and automatic centering protection mechanisms to improve system stability and safety.

The main contributions of this work are as follows:

1. A Practical Experimental Platform: A compact, low-cost, and physically validated ramp-based AUV recovery platform is developed. The system avoids the complexity and high cost of traditional stabilization platforms [9,14] while offering strong replicability.
2. Integrated Actuation and Control Design: A dual-motor wire-driven mechanism is combined with closed-loop control to achieve real-time roll and pitch compensation.
3. Midpoint Tracking Compensation Strategy: A simple and effective method is proposed to maintain the spatial alignment of the recovery window by tracking its midpoint based on real-time attitude feedback.
4. Robustness and Safety Features: Multi-level software limits and automatic centering routines are implemented to prevent faults and ensure safe operation.
5. Experimental Validation Beyond Simulation: A series of physical tests under different control parameters and disturbances confirms the system's ability to stabilize window attitude and maintain alignment. These results demonstrate the platform's effectiveness beyond purely simulation-based studies [16–18].

Compared with previous systems that either rely on complex multi-DOF mechanisms or remain untested in physical environments, the proposed approach provides a verified and scalable solution. It achieves active attitude compensation and improves docking reliability under realistic sea conditions.

The remainder of this paper is organized as follows. Section 2 presents the design of the AUV recovery platform and illustrates the working principle of the compensation mechanism. Section 3 describes the modeling and implementation of the control system. Section 4 introduces the experimental setup and testing procedures. Section 5 analyzes the experimental results and evaluates the system performance. Finally, Section 6 concludes the paper.

## 2. Ramp-Based AUV Recovery System and Compensation Principle

### 2.1. Overall Structure of the Ramp-Based AUV Recovery System

The ramp-based AUV recovery system primarily consists of the ramp body, power drive module, capture platform, compensation mechanism, attitude sensing unit, and main control unit. The overall system design builds upon our team's previous implementation of an inclined sliding-rail AUV recovery platform [9], while this study specifically focuses on the compensation mechanism installed at the rear end of the capture platform.

The inclination of the ramp is adjusted through electric pushrods mounted between the ramp structure and the base platform. By controlling the pushrod extension, the ramp can tilt into the water for AUV recovery or retract to its stowed position after completing the operation. A base sliding platform equipped with stepper motors enables the ramp to move forward and backward along the vessel deck, allowing precise positioning of the recovery interface relative to the approaching AUV. The energy module is integrated at the top of the structure, providing a self-contained power source for the entire system without requiring external wiring.

The capture platform is mounted at the rear of the ramp body and serves as the docking interface for the AUV. A triangular capture window is formed by a horizontally tensioned recovery cable connected to the winch at the front and lateral wire ropes on both sides. The rope-tensioning mechanism, symmetrically arranged along the platform, maintains the spatial geometry and tension of the capture window, ensuring its stability under wave-induced disturbances. During recovery operations, the AUV approaches the stern of the vessel and engages the capture window using a passive latching device mounted at its bow, initiating the docking sequence. The overall structure of the system is illustrated in Figure 1.

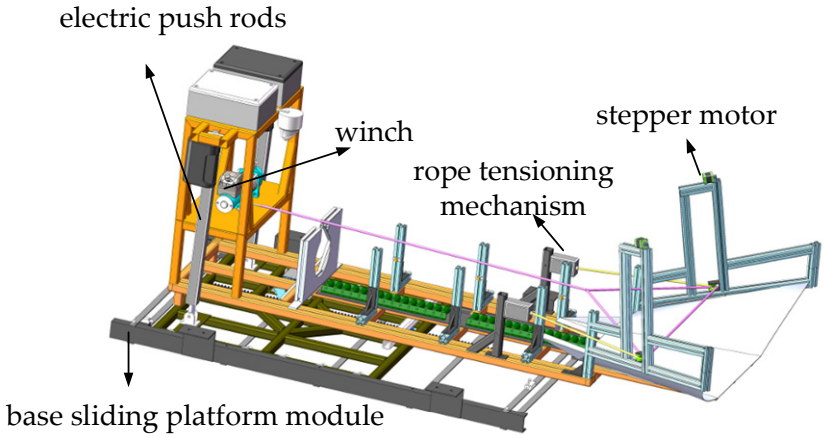



**Figure 1.** Overall structure of the ramp-based AUV recovery system.

This paper focuses on the design and experimental verification of the compensation mechanism located at the rear end of the capture platform. The remaining structural components and operational workflow largely follow the team's previous work and will not be elaborated here. In real marine environments, the ramp platform and its capture window are highly susceptible to multi-degree-of-freedom attitude disturbances that adversely affect the safety and docking success rate of the recovery process [23].

The core structure of the ramp-based AUV recovery system is illustrated in Figure 2. At the front end of the system, a triangular capture window is formed by the capture rope, which is connected to the winch and the lateral wire ropes on both sides. This configuration enables the active capture and guidance of the AUV. The spatial configuration and tension of the capture window are dynamically regulated by the wire ropes driven by

two independent motors on both sides. This dynamic adjustment ensures that the capture window maintains a stable geometry under wave disturbances [24], providing a reliable entrance for AUV recovery.

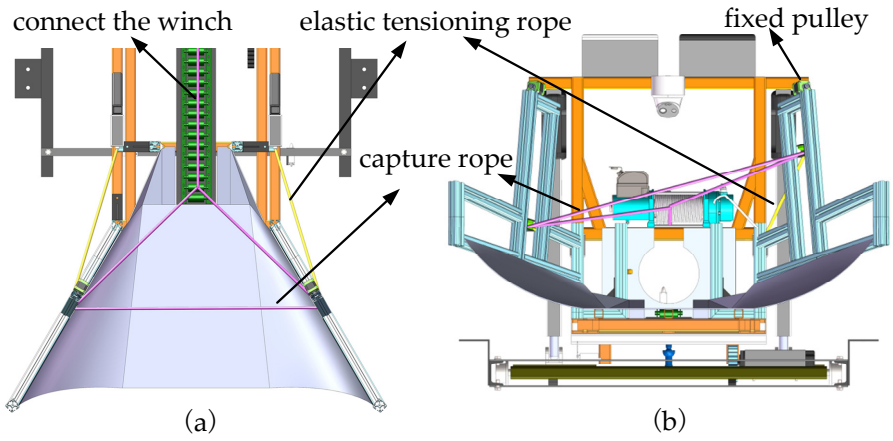



**Figure 2.** Structural diagrams of the capture window and compensation mechanism: (**a**) Top view showing the triangular capture rope and winch connection; (**b**) Front view illustrating the tensioning system and platform arrangement.

In actual operations, the AUV is typically equipped with a dedicated latching mechanism at its front, which must accurately engage the capture rope at the leading edge of the window to initiate the recovery sequence. If the leading edge of the capture window cannot maintain a horizontal alignment or it drifts vertically, the latching mechanism may fail to engage, resulting in docking failures. Therefore, maintaining the horizontal orientation and constant height of the capture rope at the window's leading edge is critical for improving the success rate, safety, and operational reliability of the AUV autonomous docking process. The primary objective of the compensation mechanism designed in this study is to achieve real-time adjustment of the capture window's attitude, ensuring that the capture rope remains in the ideal spatial position under various disturbances and maximizing the success of AUV docking.

Through the coordinated action of the lateral wire ropes and the end-tensioning mechanism, the platform can automatically adjust the height of both sides of the window based on real-time attitude feedback of roll and pitch angles, thereby dynamically compensating for roll and pitch disturbances [16]. As a result, even under complex sea conditions, the recovery window remains aligned with the AUV docking window, significantly enhancing operational safety and docking success rates.

### *2.2. Structure and Working Principle of the Compensation Mechanism*

#### 2.2.1. Coordinate System and Attitude Definition

To describe the spatial attitude of the recovery window, a coordinate system is established, as illustrated in Figure 3. The X-axis is aligned with the extension direction of the ramp, the Y-axis is oriented laterally across the ramp, and the Z-axis points vertically downward. The roll angle of the capture platform is defined as the rotation around the X-axis, while the pitch angle is defined as the rotation around the Y-axis. Both roll and pitch angles are continuously measured in real time by the attitude sensor [25].

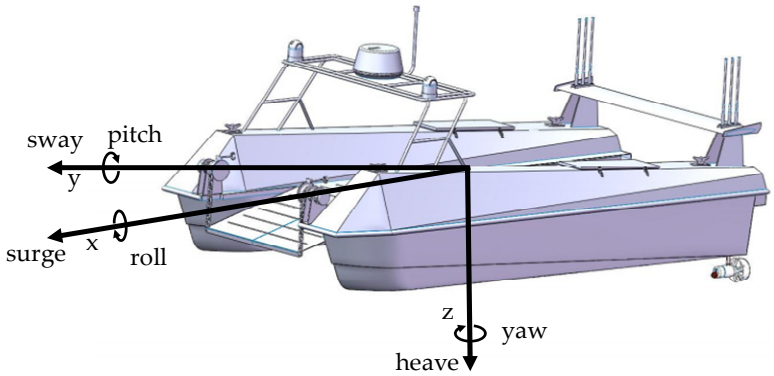



**Figure 3.** Coordinate system and attitude definition of the capture platform.

### 2.2.2. Implementation of Roll and Pitch Compensation

The compensation mechanism adopts a dual-motor wire-driven structure, in which the left and right motors respectively control the elevation of the wire ropes attached to both sides of the capture window, thereby enabling dynamic compensation for both roll and pitch attitudes of the platform [26]. Specifically, each motor drives a fixed pulley installed on the corresponding side of the capture platform. A pair of elastic tensioning ropes are arranged symmetrically, routed through the fixed pulleys, and connected to the ends of the central recovery rope that forms the triangular capture window. By adjusting the vertical position of the fixed pulleys, the system indirectly alters the length and tension distribution of the elastic ropes, dynamically modifying the spatial orientation of the capture window while preserving its geometric stability.

When roll disturbances are detected by the attitude sensor, the main control unit calculates the differential displacements for the two motors, causing the left and right fixed pulleys to move in opposite directions. This effectively rotates the capture window around its longitudinal axis, restoring the horizontal orientation and aligning the platform's roll angle with the target reference. In response to pitch disturbances, both motors are synchronously adjusted to modify the overall height of the capture window, thus compensating for pitch deviations. This mechanism allows real-time adaptation to external disturbances, significantly improving the spatial attitude stability of the AUV recovery window.

The core compensation principle is illustrated in Figure 4 and expressed as:

$$\theta_{win} + \theta_{roll} = 0 \tag{1}$$

where $\theta_{win}$ represents the tilt angle of the capture window, and $\theta_{roll}$ is the roll angle of the platform.

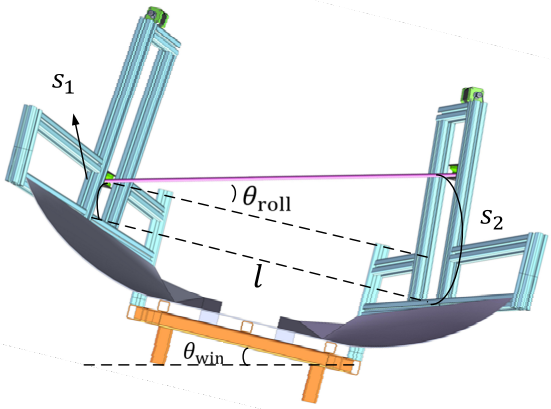



**Figure 4.** Geometric principle of roll compensation for the capture window.

For pitch disturbance compensation, the system dynamically calculates the target height of the capture window's midpoint based on the real-time pitch angle measured by the attitude sensor and the geometric parameters of the window [27]. The main control unit synchronously adjusts the elevation of both motors to ensure that the midpoint of the window accurately tracks the calculated target value. When the bow pitches downward (positive pitch angle), the system automatically raises both wire rope ends, lifting the entire capture window; conversely, when the pitch angle is negative, the system lowers both sides to compensate accordingly. This strategy effectively offsets the vertical displacement of the capture window induced by vessel pitch motions, thereby maintaining spatial alignment between the recovery window and the AUV docking trajectory, and improving docking stability and compensation performance.

The operational side view of the recovery vessel is shown in Figure 5a, and the simplified geometric model for pitch compensation is illustrated in Figure 5b.

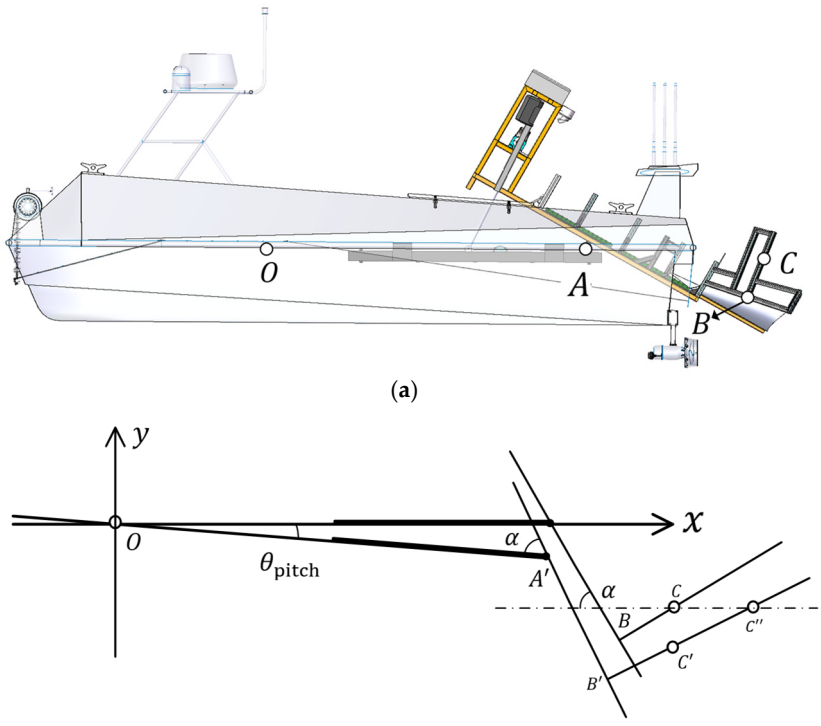



**Figure 5.** Geometric diagrams for pitch compensation: (**a**) Side view of the recovery vessel during operation; (**b**) Simplified geometric model for pitch disturbance compensation.

Let point $O$ denote the rotational center of the vessel during pitch motion, and point $C$ represent the midpoint position of the two wire ropes. The pitch angle is denoted as $\theta_{pitch}$, and the inclined angle of the recovery ramp in its working state is defined as $\alpha$. The initial coordinates of points $B$ and $C$ are expressed as $(x_B, y_B)$ and $(x_C, y_C)$, respectively.

Under pitch motion, the coordinates of points $B'$ and $C'$, after rotating around point $O$ by an angle $\theta_{pitch}$, can be obtained using the standard planar rotation transformation [5]:

$$\begin{bmatrix} x' \\ y' \end{bmatrix} = \begin{bmatrix} cos\theta_{pitch} & -sin\theta_{pitch} \\ sin\theta_{pitch} & cos\theta_{pitch} \end{bmatrix} \begin{bmatrix} x \\ y \end{bmatrix} \tag{2}$$

Accordingly, the rotated coordinates of points $B'$ and $C'$ are given by:

$$\begin{aligned} x\prime_B &= x_B cos\theta_{pitch} - y_B sin\theta_{pitch} \\ y'_B &= x_B cos\theta_{pitch} + y_B sin\theta_{pitch} \\ x'_c &= x_c cos\theta_{pitch} - y_c sin\theta_{pitch} \\ y'_c &= x_c cos\theta_{pitch} + y_c sin\theta_{pitch} \end{aligned} \tag{3}$$

The straight-line equation of segment $B'C'$ can be expressed as:

$$y = \frac{y'_B - y'_C}{x'_B - x'_C}(x - x'_B) + y'_C \tag{4}$$

To compute the vertical displacement of point $C$, its projected coordinate along line $B'C'$, denoted as $C''$, is calculated. The coordinates of $C''$ are given by:

$$\begin{aligned} x''_C &= x_C \\ y''_C &= \frac{y'_B - y'_C}{x'_B - x'_C}(x_C - x'_B) + y'_C \end{aligned} \tag{5}$$

Finally, the compensation length $L$, which represents the vertical deviation of point $C$ under pitch disturbances, is obtained as:

$$L = \sqrt{(x'_B - x''_C)^2 + (y'_B - y''_C)^2} \tag{6}$$

Based on the above derivation, the system dynamically calculates the target height of the capture window midpoint according to the real-time pitch angle measured by the attitude sensor and the platform's structural parameters [28], thereby achieving accurate pitch compensation during vessel motion. This strategy effectively offsets the vertical displacement of the capture window induced by pitch disturbances, maintaining spatial alignment between the recovery window and the AUV docking trajectory.

It is acknowledged that in real marine environments, the vertical position of the capture window's midpoint is affected by both pitch and heave motions. The proposed compensation mechanism can theoretically adjust the midpoint height through synchronized actuation of both motors. However, actual heave-induced vertical displacement is not considered in this study due to the lack of dedicated heave measurement devices in the current setup.

Translational disturbances such as surge, sway, and heave are typically managed by the AUV's own positioning and motion control capabilities during docking. In contrast, attitude disturbances, especially roll and pitch variations of the recovery window, are more difficult for the AUV to perceive and compensate for. This is due to the limited roll and pitch control authority of most AUV platforms. Therefore, this study focuses on actively compensating for roll and pitch disturbances using the proposed mechanical mechanism. In future work, heave sensing and control will be incorporated to further enhance the compensation performance and improve overall docking stability under complex sea conditions.

## 3. Control System Implementation

### *3.1. Overall Control Architecture*

To achieve real-time compensation of the capture window's attitude in the ramp-based AUV recovery system, a closed-loop control system based on attitude feedback is designed in this study. As illustrated in Figure 6, the system consists of three main components: a sensing unit, a control unit, and an actuation unit.

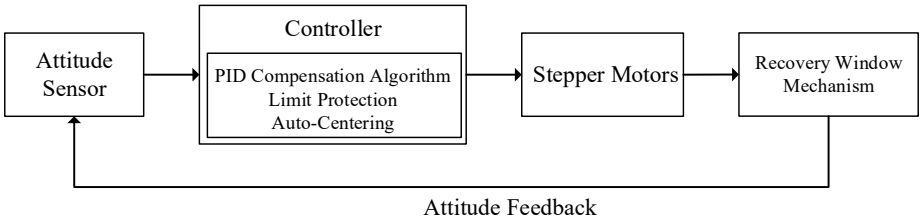



**Figure 6.** Signal flow diagram of the closed-loop control system for the ramp-based AUV recovery platform.

The sensing unit is responsible for real-time acquisition of the roll and pitch angles of the capture window. A high-precision attitude sensor is used to obtain the current spatial attitude of the platform. The control unit, centered on an embedded controller, continuously receives attitude signals and computes the real-time deviation between the current and target attitudes of the capture window. Based on this error, it dynamically generates control commands for the left and right motors.

The actuation unit consists of two wire-driven motors and their corresponding drive circuits. In response to the commands from the control unit, the left and right motors adjust the lengths of the wire ropes to achieve differential tilt for roll compensation and synchronized elevation for pitch compensation, respectively. This allows for real-time adjustment of the spatial orientation of the recovery window. When roll or pitch disturbances are detected on the mother vessel, the controller calculates and corrects the rope heights in real time, ensuring that the capture window remains level with the sea surface and aligned with the AUV docking trajectory.

To ensure operational safety, the control system is equipped with stroke limit protection and fault detection mechanisms. In cases of overextension, component failure, or other abnormal conditions, the system can automatically halt actuator movement to prevent structural damage.

Overall, the control system forms a closed-loop architecture encompassing sensing, decision-making, actuation, and feedback. It enables dynamic adjustment and stable compensation of the platform's attitude. The system features fast response, high control precision, and straightforward implementation, and it is equipped with comprehensive safety protection measures. These characteristics significantly enhance the operational reliability of the platform and provide strong technical support for safe and efficient AUV recovery under complex sea conditions.

### *3.2. Key Hardware and Software Implementation*

The hardware implementation of the compensation control system primarily consists of an industrial control host, an attitude sensor, stepper motors and drivers, power supply modules, and other supporting components. The detailed connection layout is shown in Figure 7.

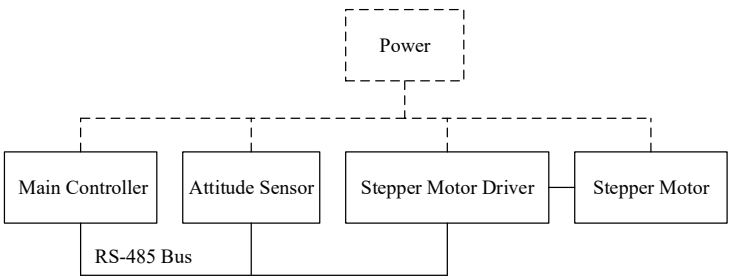



**Figure 7.** Hardware connection diagram of the compensation control system based on an industrial PC and RS-485 bus.

The hardware architecture adopts an RS-485 bus structure for stable and reliable communication between the controller and peripheral devices. The industrial control host functions as the central processing unit, which collects real-time attitude data from the sensor, executes the compensation algorithm, and sends control commands to the stepper motor drivers. The power supply modules provide a stable operating voltage for each unit, ensuring system functionality under varying load conditions.

Due to the current development stage, prototype verification of key components was conducted using a desktop experimental platform. The technical specifications and physical structure of the hardware used for experimental validation are presented in Section 4.1. The experimental hardware configuration maintains functional consistency with the overall system design shown in Figure 7, ensuring that the prototype performance reflects the practical feasibility of the proposed compensation system.

The software implementation of the compensation control system consists of several key functional modules, including attitude data acquisition and processing, control algorithm execution and command output, motor actuation control, data logging and communication, as well as limit protection and fault handling. The detailed software workflow is illustrated in Figure 8.

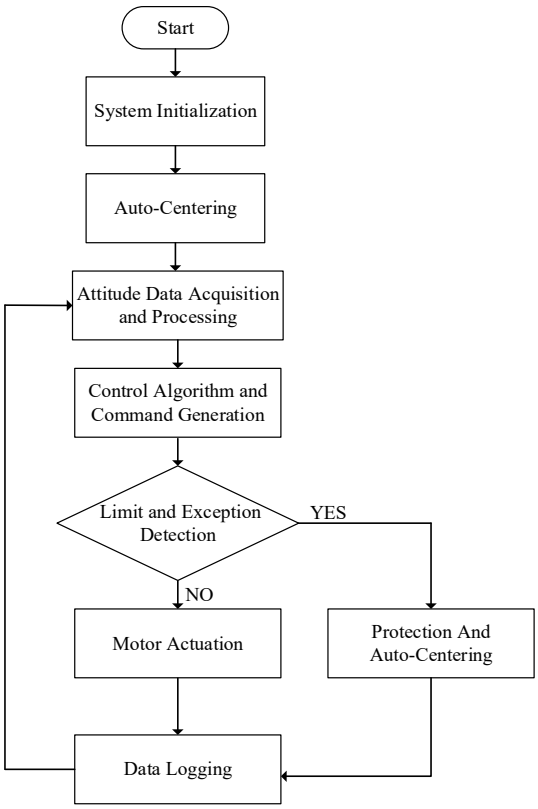



**Figure 8.** Software flowchart of the compensation control system.

At system startup, the controller initializes all sensors, communication interfaces, and motor drivers to ensure operational readiness. The platform then enters an automatic centering mode, driving the capture window to its default neutral position.

Once initialized, the system continuously acquires roll and pitch attitude data from the onboard sensor. These measurements are directly used as input for real-time closed-loop control. The control algorithm compares the measured attitude with the desired reference, calculates the error, and generates motor commands. Differential motor adjustments compensate for roll disturbances, while synchronized adjustments correct pitch deviations. A PID control strategy ensures fast, stable attitude correction under external disturbances.

The system includes a limit protection and fault detection module. It monitors motor displacement, rope tension, and component status. If an overextension, mechanical jam, or sensor failure is detected, the system halts actuation and triggers automatic centering to reset the platform safely.

During normal operation, the motor control module adjusts the recovery window in real time. Meanwhile, the data logging module records key parameters, such as attitude angles, motor status, and fault events. These records support performance evaluation and fault diagnostics.

This structured software design ensures reliable, real-time attitude compensation. Integrated safety functions enhance system protection and operational stability.

### *3.3. System Modeling and Control Principle*

#### 3.3.1. Stepper Motor Model and PWM Pulse Control

To represent the electromechanical dynamics of the actuation system, the stepper motor is modeled as a two-phase hybrid motor. The governing equations are:

$$\dot{\theta} = \omega \tag{7}$$

$$\dot{\omega} = \frac{1}{J}[-K_m i_A \sin(p\theta) + K_m i_B \cos(p\theta) - B\omega - \tau_1] \tag{8}$$

$$\dot{i}_A = \frac{1}{L}[v_A - Ri_A + K_m \omega \sin(p\theta)] \tag{9}$$

$$\dot{i}_B = \frac{1}{L}[v_B - Ri_B + K_m \omega \cos(p\theta)] \tag{10}$$

where, $i_A$ and $i_B$ represent the currents of phase A and phase B, respectively; $v_A$ and $v_B$ represent the voltages of phase A and phase B, respectively; $\theta$ and $\omega$ are the angle and angular acceleration, respectively; $B$ is the viscous friction coefficient; $J$ is the moment of inertia of the motor; $K_m$ is the motor torque constant; $R$ and $L$ are the phase resistance and phase inductance, respectively; $p$ is the number of rotor poles; and $\tau_1$ is the load torque.

Given the strong nonlinearity of the mathematical model, a practical pulse control strategy is adopted for real-time stepper motor control. The control system employs a standard open-loop subdivision drive, where the controller generates pulse signals corresponding to the desired target position. These pulses are then transmitted to the motor driver, which activates the two-phase windings of the stepper motor accordingly.

The overall PWM pulse control framework is illustrated in Figure 9, which includes the target position input, controller, stepper motor driver, motor, and rotary encoder for position feedback.

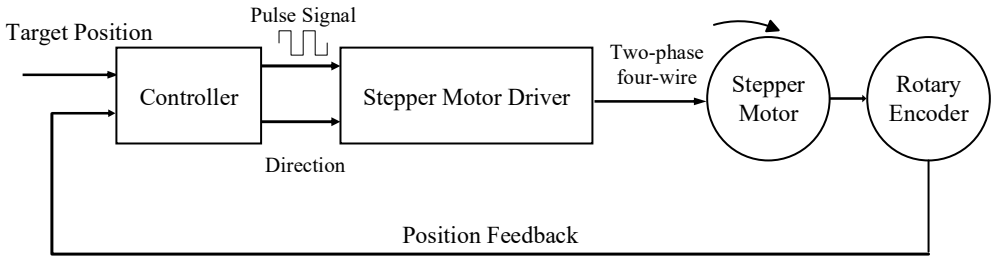



**Figure 9.** PWM pulse control diagram of the stepper motor system.

As shown in Figure 9, the controller generates pulse signals based on the target position. The driver uses these signals to excite the motor's two-phase windings in sequence. This pulse-based control simplifies the nonlinear dynamics and ensures precise tracking.

For a motor with $p$ rotor poles and $N_{sub}$ subdivisions, the step angle is:

$$\theta_s = \frac{2\pi}{n_{ph} p N_{sub}} \tag{11}$$

where $\theta_s$ is the step angle per pulse, and $n_{ph}$ is the number of phases. When the pulse frequency is $f_{pwm}$, the resulting motor speed can be expressed as:

$$|\omega| = \frac{2\pi f_{pwm}}{n_{ph} p N_{sub}} = \theta_s f_{pwm} \tag{12}$$

Thus, motor speed is directly proportional to pulse frequency. Adjusting the pulse rate allows precise control of the compensation mechanism. To support system analysis and controller implementation, the following section introduces a simplified dynamic model and the corresponding PID-based control approach.

#### 3.3.2. First-Order System Approximation and PID Control

To analyze the dynamic response characteristics of the compensation platform, the system simplifies the process from motor input to slider displacement as a first-order linear system. The corresponding transfer function in the Laplace domain is given by:

$$G(s) = \frac{X(s)}{U(s)} = \frac{r_0 \theta_s}{\tau s + 1} \tag{13}$$

where $X(s)$ and $U(s)$ are the Laplace transforms of the actual slider displacement and the motor control input signal, respectively. $\theta_s$ represents the motor step angle, $r_0$ is the proportional coefficient relating motor rotation to platform displacement, and $\tau$ is the system time constant.

To perform roll and pitch attitude compensation, the platform calculates the target displacements of the left and right sliders in real time based on the attitude angles measured by the attitude sensor and the geometric relationships described in Section 2.2. Since the control algorithm is implemented on a digital industrial controller operating at 20 Hz, the PID controller is realized in discrete-time form with a fixed sampling time of $T_s = 10$ ms. The control signal at time step $k$ is given by [29]:

$$u[k] = K_p e[k] + K_i \sum_{i=0}^{k} e[k] T_s + K_d \frac{e[k] - e[k-1]}{T_s} \tag{14}$$

where $u[k]$ is the control output (motor command), $e[k]$ is the attitude error between the reference and measured values, $K_p$, $K_i$, and $K_d$ are the proportional, integral, and derivative gains, respectively, and $T_s$ is the control sampling time.

This discrete implementation ensures compatibility with the real-time control system and supports stable operation under periodic updates. Since the stepper motors are driven via open-loop PWM frequency and the belt transmission introduces minimal elasticity or inertia, the actuation dynamics approximate a first-order system. This simplification is appropriate for the platform's low-frequency operation and lightweight structure, where high-order dynamics are negligible.

Although this model does not account for effects such as belt elasticity or mechanical backlash, experimental results show that the simplified approach provides adequate accuracy for real-time compensation. More detailed system identification can be considered in future studies if higher robustness is required. From a design perspective, the discrete PID structure combined with saturation protection and re-centering logic is expected to provide bounded and stable responses under nominal operating conditions.

In addition to the primary PID controller, a secondary PID loop ensures symmetry between the two sliders. This prevents drift and keeps the capture window centered within the guide rail. When either slider approaches a physical or software-defined limit, the system interrupts normal control and enters a re-centering mode. During this mode, both sliders are driven toward the rail's midpoint. Once the system returns to the safety zone, normal compensation resumes.

This multi-layered control and protection scheme helps prevent structural overextension and enhances system robustness and autonomy during experimental operation.

### *3.4. Control System Workflow*

As shown in Figure 10, the overall workflow of the compensation control system includes system startup, attitude acquisition, error calculation, control decision-making, actuator execution, safety protection, and data logging. The process proceeds as follows:

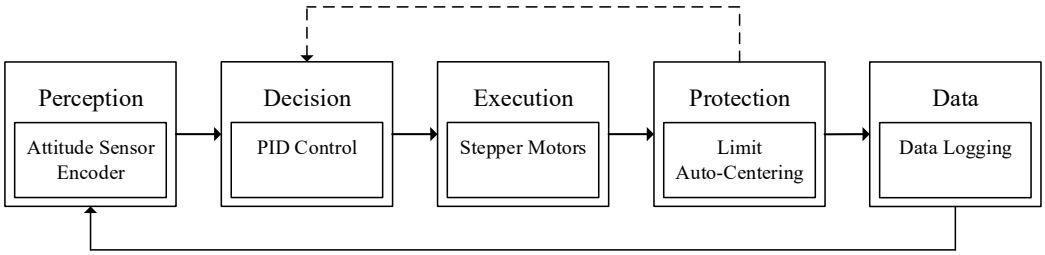



**Figure 10.** Block diagram of the overall closed-loop control workflow for the compensation system.

Upon powering on, the main control unit initializes and performs self-checks on key hardware components, including the attitude sensor, left and right motors, and limit switches, to ensure that all the modules are properly connected and operational. Once initialization is complete, the system enters the closed-loop control cycle.

During normal operation, the attitude sensor continuously acquires the roll and pitch angles of the capture window. The main controller periodically reads and parses attitude sensor output to obtain real-time attitude information. This is followed by a comparison between the current window attitude and the target reference, and the resulting attitude error is calculated. Based on the error, the PID control algorithm is executed to generate control commands for both motors, including direction and speed.

The left and right motors respond to the commands by adjusting the wire rope lengths accordingly, enabling either independent or synchronized elevation of the window ends to compensate for roll and pitch disturbances. While adjusting the platform attitude, the main controller continuously monitors the status of the limit switches and motor operating conditions. If the system detects that a motor has reached its mechanical limit or encounters a fault condition (such as motor overload or attitude sensor failure), it immediately triggers safety protocols, including motor shutdown, alarm notification, or automatic re-centering of the window.

Throughout the control cycle, the system also logs key operational data, such as window attitude, motor status, and control outputs. These records are stored locally on the industrial controller for subsequent data analysis and system optimization.

## 4. Experimental Platform and Test Methodology

### *4.1. Experimental Platform Setup and Key Parameters*

To evaluate the attitude compensation performance of the proposed mechanism, a desktop-scale physical test platform for recovery compensation was constructed, as shown in Figure 11. The platform mainly consists of a dual-slider rail support structure, left and

right stepper motors, wire encoders, a capture window tensioning mechanism, an attitude sensor, a main control unit, and a limit protection module.

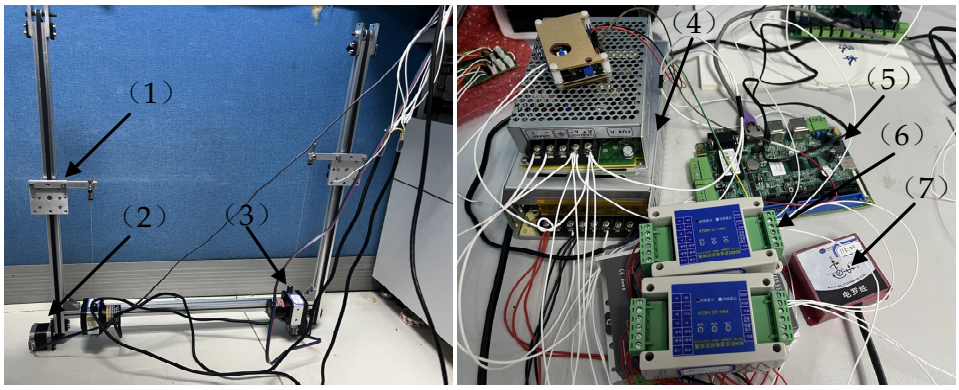



**Figure 11.** Labeled photograph of the experimental platform: (1) Linear slider; (2) Stepper motor; (3) Wire encoder; (4) Power supply module; (5) Industrial control board; (6) Stepper motor driver; (7) Attitude sensor.

The platform is a scaled desktop model designed for compensation testing. It features a dual-slider rail structure with a travel range of 40 cm and a spacing of 50 cm. Both rails are constructed from aluminum profiles and mounted on opposite sides of a desktop frame, ensuring stable motion of the capture window. Each side is equipped with a 42-series stepper motor, which adjusts the height of the window ends via timing belts, enabling either independent or synchronized elevation. In combination with wire encoders, the system provides real-time feedback on the positions of both sliders, forming a closed-loop control system.

The structure of the capture window adopts the triangular rope-tensioning scheme developed in the team's earlier work. The ends of the window are tensioned by springs and winch mechanisms connected to the wire ropes, maintaining tension and spatial configuration under disturbances. Unlike the previous system, which relied solely on passive tensioning, the platform introduced in this study innovatively integrates dual-slider rails and motor-driven actuation, enabling active height adjustment and providing the capability to compensate for both roll and pitch motions.

The core control unit of the platform is an EPC-9600 industrial control board, which collects attitude information from the PM-C3000 electronic compass. The PM-C3000 is equipped with a three-axis magnetometer and a three-axis accelerometer, without an integrated gyroscope. As a result, this module does not provide complete inertial measurement data. Nevertheless, it allows reliable real-time acquisition of roll and pitch angles, which satisfies the requirements for attitude sensing in this desktop-scale compensation experiment.

The platform features a compact structure and comprehensive functionality, serving as a testbed for evaluating the actuation performance and control strategy of the compensation mechanism. The main parameters of the platform are listed in Table 1.

**Table 1.** Main components and specifications of the experimental platform.

| Component | Specification/Model | Description |
|---|---|---|
| Platform | 40 cm × 50 cm | Desktop-scale scaled platform |
| Slider structure | Aluminum profiles, belt | Dual-sided linear guide rails |
| Stepper motor | 42-series stepper motors | Dual-sided actuation of sliding platform |
| Attitude sensor | PM-C3000 | Real-time roll and pitch acquisition |
| Control unit | EPC-9600 industrial board | Data processing and motor control |
| Position sensing | Wire encoder | Feedback on capture rope displacement |
| Power supply | AC adapter | Desktop power supply |

To enhance the practicality and efficiency of the experimental platform, each hardware component was selected based on its performance, cost, and suitability for desktop-scale prototyping. The EPC-9600 industrial control board, running an embedded Linux system, offers reliable real-time processing and high compatibility with sensor and actuator interfaces, making it suitable for rapid development and integration of the control logic. The PM-C3000 electronic compass was chosen primarily for its compact size, ease of integration, and compatibility with the EPC-9600 control board. Its magnetometer–accelerometer configuration allows direct extraction of roll and pitch without requiring complex filtering or sensor fusion algorithms, simplifying system implementation.

The actuation system employs a pair of 42-series stepper motors coupled with timing belt-driven linear sliders on each side. This configuration provides fast and smooth motion, and its open-loop control capability simplifies implementation. Compared to screw-based actuators, belt-driven sliders offer higher speeds and are more appropriate for the rapid adjustments required in dynamic compensation. Wire encoders are used for position feedback of the sliders, enabling closed-loop control and ensuring accurate tracking of the compensation trajectory. The overall design prioritizes low cost, ease of implementation, and reliable motion performance, which aligns with this study's goal of developing a compact, replicable recovery compensation mechanism.

In addition to the desktop platform, a USV platform was utilized for real-world sea condition data collection. As shown in Figure 12, the attitude sensor was mounted on the deck of the USV to continuously capture roll and pitch variations induced by environmental disturbances or intentional excitation during controlled tests. The collected attitude data were then transmitted to the compensation system for real-time or offline playback experiments, enabling comprehensive evaluation of the compensation mechanism's performance under realistic disturbance conditions.




**Figure 12.** Photograph of the USV platform used for attitude disturbance data collection.

### 4.2. Experimental Conditions and Procedure Design

To simulate the attitude disturbances experienced by a vessel in wave environments, two data acquisition and disturbance reproduction methods were designed to evaluate the dynamic response and compensation performance of the system. The attitude sensor used in this study reflects the spatial attitude of the recovery platform, representing the roll and pitch disturbances acting on the capture window. This setup provides a controllable and reliable approach for testing the compensation system under laboratory and semi-physical conditions.

1. Real-Time USV Disturbance Test: The attitude sensor was mounted on the USV deck to continuously collect roll and pitch variations induced by intentional excitation or the vessel's own motion, simulating typical sea conditions. The compensation system, deployed onshore or on the USV deck in a safe area, received real-time attitude data and dynamically adjusted the compensation mechanism for real-time attitude correction.
2. Offline Playback Test Using USV Measured Data: Attitude disturbance data were collected from the USV under controlled wave conditions in a water tank. The recorded data were stored and repeatedly loaded into a desktop platform for closed-loop compensation tests.

The compensation system followed the same operational procedure under both test scenarios, as illustrated in Figure 13.

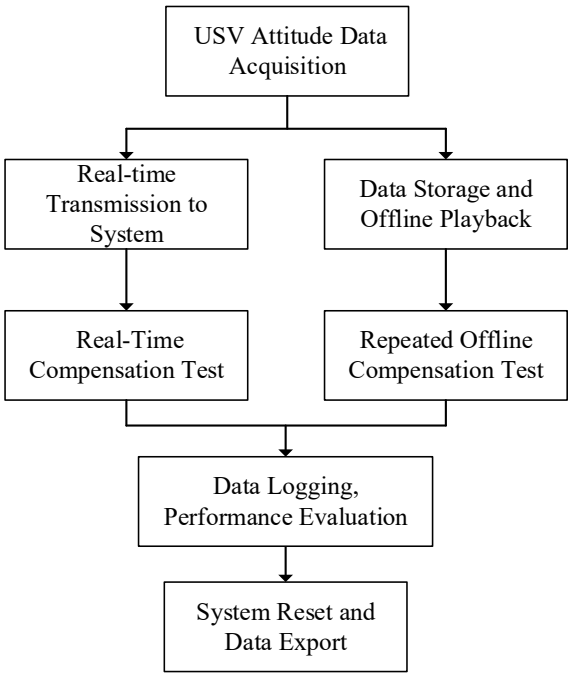



**Figure 13.** Experimental procedure flowchart.

The main control unit calculated the attitude error based on the target attitude information and dynamically drove the left and right stepper motors to adjust the compensation mechanism, correcting the orientation of the capture window. During the experiment, the system continuously logged key data, including the target attitude, actual window attitude, compensation response, and motor status. To comprehensively evaluate the compensation performance, multiple disturbance scenarios with varying amplitudes, frequencies, and durations were configured, incorporating both roll and pitch disturbances. Comparative tests were conducted with and without compensation. Each test was repeated multiple times to ensure data reliability and result repeatability. After the experiment, the compensation

mechanism automatically returned to its initial (centered) position, and all the recorded data were exported for subsequent analysis and performance evaluation.

### 4.3. Data Acquisition and Processing Method

During each test cycle, the system continuously acquires key parameters, including platform attitude, compensation actuation, and control status. The attitude sensor samples and outputs real-time roll and pitch angles, while the main control unit generates control signals at a frequency of 100 Hz and simultaneously records the target angle, actual midpoint height, motor displacements, wire rope lengths, and limit switch states. All experimental data are stored in CSV format on the industrial controller and later uploaded to a host computer for analysis.

The attitude information utilized in this study is obtained from the PM-C3000 electronic compass, which integrates a three-axis magnetometer and a three-axis accelerometer. The sensor incorporates built-in hard and soft magnetic field calibration, tilt compensation, and temperature compensation algorithms to enhance measurement stability. The output signals include optimized magnetic field, acceleration, and temperature data, which are used to estimate roll and pitch angles in real time. No additional filtering or sensor fusion algorithms beyond the manufacturer's internal compensation were applied during the experiments. Considering the controlled conditions and low dynamic disturbances of the desktop-scale platform, the current attitude acquisition configuration provides sufficient accuracy for platform-level attitude compensation. Nevertheless, to further improve system performance under more complex environmental conditions, future studies will incorporate complete inertial measurement units with integrated gyroscopes and advanced filtering techniques to enhance attitude estimation accuracy and dynamic disturbance rejection capability.

To ensure data accuracy and reliability, repeated measurements were conducted under each test condition. Key experimental data were post-processed using MATLAB R2024b, including outlier removal, curve smoothing, and signal alignment. Based on the processed data, the following performance evaluation metrics were defined:

1. Attitude tracking error: This metric quantifies how accurately the platform tracks the target attitude provided by the attitude sensor. It is evaluated using mean squared error ($MSE$) and maximum absolute error ($MaxAE$), defined as follows [30]:

$$MSE = \frac{1}{N}\sum_{i=1}^{N}\left(\theta_{act}(i) - \theta_{ref}(i)\right)^2 \tag{15}$$

$$MaxAE = \max_{i}\left|\theta_{act}(i) - \theta_{ref}(i)\right| \tag{16}$$

where $\theta_{act}(i)$ and $\theta_{ref}(i)$ represent the actual and reference angles, respectively, at time step $i$, and $N$ is the total number of samples.

$MSE$ reflects the overall stability of attitude tracking over time, while $MaxAE$ captures the worst-case deviation, indicating the system's ability to reject sudden disturbances

2. System response delay: This metric reflects the real-time responsiveness of the platform. Cross-correlation analysis is used to evaluate the time delay between the reference and actual angle sequences. The delay corresponding to the maximum value of the cross-correlation function is taken as the average system response delay:

$$T_{delay} = \tau_{max} \times \Delta t \tag{17}$$

where $\Delta t$ is the sampling interval, and $\tau_{max}$ is the lag corresponding to the maximum cross-correlation. The cross-correlation function is defined as [31,32]:

$$C(\tau) = \sum_{i=1}^{N-\tau} \left(\theta_{ref}(i) - \overline{\theta_{ref}}\right) \cdot \left(\theta_{act}(i+\tau) - \overline{\theta_{act}}\right) \quad (18)$$

where $\tau$ is the lag in samples, and $\overline{\theta_{ref}}$ and $\overline{\theta_{act}}$ are the mean values of the corresponding sequences.

3. Tracking performance under coupled disturbances: Evaluated using $MSE$, $MaxAE$, and response delay in single-run tests with simultaneous roll and pitch excitation. These metrics characterize the system's dynamic accuracy and responsiveness under multi-degree-of-freedom conditions.

All collected data and evaluation results are used in the following sections for comparative analysis and system performance assessment.

## 5. Experimental Results and Analysis

### *5.1. Controller Parameter Tuning and Comparative Test*

#### 5.1.1. PD vs. PID Controller Performance Comparison

To investigate the influence of the integral gain $K_i$ on system performance, a series of experiments was conducted with fixed proportional and derivative gains ($K_p = 3000$, $K_d = 30$) while varying $K_i$ across a representative range. For each test, the same disturbance input was applied using offline playback of USV-recorded attitude data, ensuring consistent and reproducible excitation conditions.

The experimental results are summarized in Figure 14. Subfigure (a) shows the $MSE$ and $MaxAE$ trends as $K_i$ increases, reflecting the system's tracking accuracy. Subfigure (b) presents the corresponding system delay, which remained stable across the tested range. A detailed comparison of all test cases is provided in Table 2, which lists the specific values of $K_i$, $MSE$, $MaxAE$, and average system delay for each configuration.

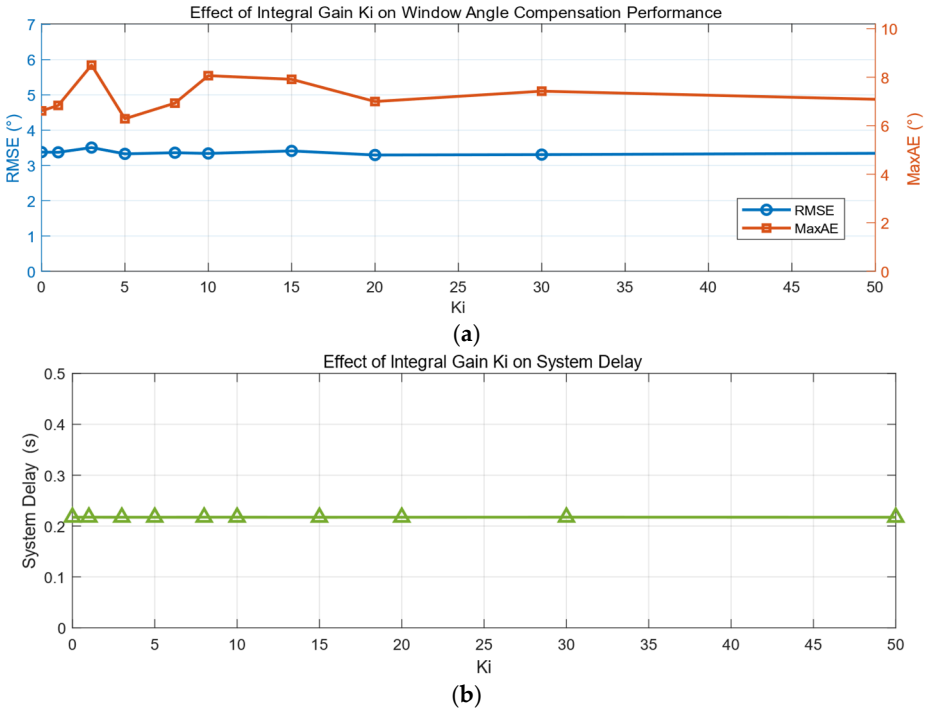



**Figure 14.** Effects of integral gain $K_i$ on compensation performance: (**a**) $MSE$ and $MaxAE$ vs. $K_i$; (**b**) System delay vs. $K_i$.

**Table 2.** Summary of performance metrics under varying $K_i$ values ($with\ K_p = 3000, K_d = 30$).

| $K_i$. | *MSE* | *MaxAE* | System Delay |
|---|---|---|---|
| 0 | 3.3785 | 6.6109 | 0.21731 |
| 1 | 3.3720 | 6.8357 | 0.21741 |
| 3 | 3.5069 | 8.4977 | 0.21730 |
| 5 | 3.3282 | 6.2863 | 0.21730 |
| 8 | 3.3606 | 6.9297 | 0.21737 |
| 10 | 3.3398 | 8.0628 | 0.21737 |
| 15 | 3.4115 | 7.9122 | 0.21737 |
| 20 | 3.2959 | 6.9966 | 0.21731 |
| 30 | 3.3069 | 7.4225 | 0.21744 |
| 50 | 3.3441 | 7.0889 | 0.21726 |

Overall, the results indicate that incorporating a small integral gain does not significantly improve tracking accuracy or reduce steady-state error in this application. The system already achieves stable and accurate compensation under PD control, with only marginal variations in $MSE$ and $MaxAE$ observed across the tested $K_i$ values. Moreover, the system delay remains largely unaffected. Considering the added complexity and potential instability from integral action, the PD controller was selected as the final control scheme due to its simplicity, robustness, and sufficient performance in the current compensation task.

5.1.2. Optimal Parameter Selection and Justification

In industrial control practice, PID controllers are often parameterized using proportional band $P$, integral time $T_i$, and derivative time $T_d$. The equivalent gain form is:

$$K_{\mathrm{p}} = \frac{100}{\mathrm{P}}, K_{\mathrm{i}} = \frac{100}{\mathrm{P}} \cdot \frac{1}{\mathrm{T_i}}, K_{\mathrm{d}} = \frac{100}{\mathrm{P}} \cdot \mathrm{T_d} \tag{19}$$

Based on this, it is common to set $T_d = T_s$, the controller sampling time, in digital implementations. This leads to a practical relationship:

$$K_{\mathrm{d}} = K_{\mathrm{p}} \cdot \mathrm{T_s} \tag{20}$$

In this study, the sampling time is 10 ms, thus the derivative gain is selected as $K_{\mathrm{d}} = 0.01 \cdot K_{\mathrm{p}}$, following common industrial guidelines [33].

To determine the optimal controller parameters for the compensation mechanism, a series of experiments was conducted by varying the proportional gain $K_{\mathrm{p}}$ under the fixed condition $K_{\mathrm{d}} = 0.01 \cdot K_{\mathrm{p}}$, as discussed above. The integral gain $K_{\mathrm{i}}$ was set to 0 to isolate the effects of proportional–derivative control.

In each test case, the same USV-recorded disturbance profile was replayed on the desktop platform, ensuring consistent and comparable excitation across different parameter settings. The system performance was evaluated in terms of $MSE$, $MaxAE$, and system response delay, which collectively reflect the tracking accuracy, stability, and responsiveness of the compensation controller.

The experimental results are presented in Figure 15, showing the $MSE$ and $MaxAE$ trends with respect to increasing $K_{\mathrm{d}}$ values. Subfigure (a) illustrates the impact on tracking error, while subfigure (b) displays the corresponding system delay. Table 3 summarizes the detailed results for all tested configurations.

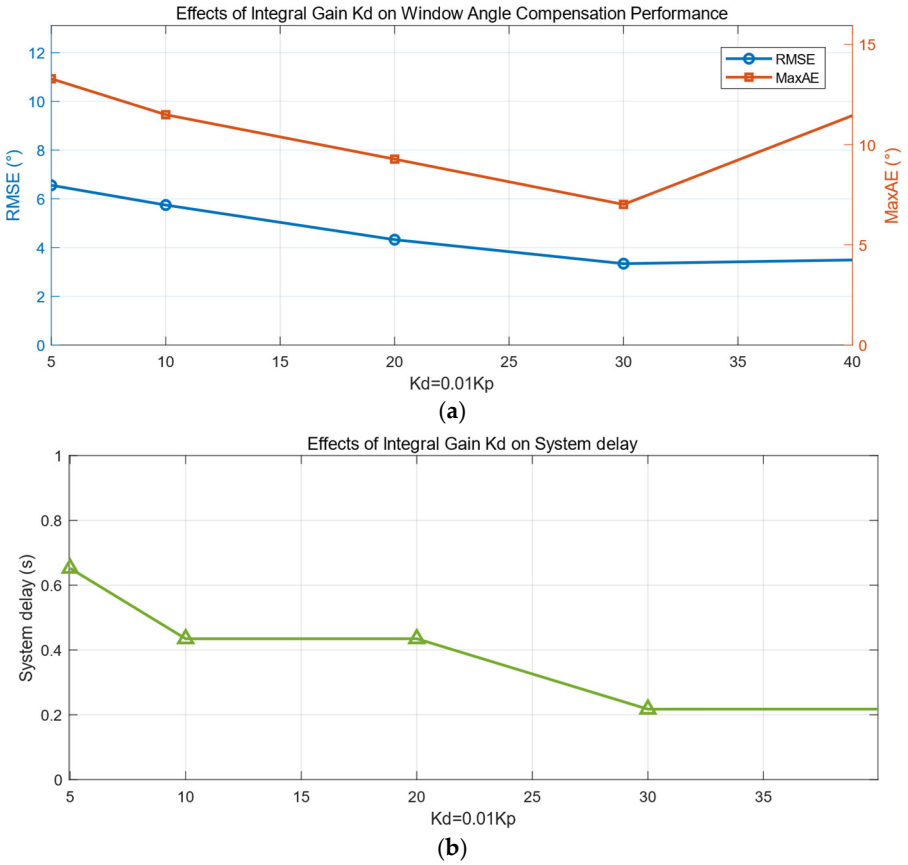



**Figure 15.** Effect of proportional gain $K_{\mathrm{d}}$ on compensation performance: (**a**) RMSE and MaxAE vs. $K_d$; (**b**) system delay vs. $K_d$ (with $K_{\mathrm{d}} = 0.01 \cdot K_{\mathrm{p}}$, $K_{\mathrm{i}} = 0$).

**Table 3.** Summary of performance metrics under varying $K_d$ values (with $K_{\mathrm{p}} = 0.01 \cdot K_{\mathrm{p}}$, $K_{\mathrm{i}} = 0$).

| $K_{\mathrm{d}}$ | *MSE* | *MaxAE* | System Delay |
|---|---|---|---|
| 5 | 6.5566 | 13.290 | 0.65214 |
| 10 | 5.7446 | 11.498 | 0.43470 |
| 20 | 4.3233 | 9.2790 | 0.43473 |
| 30 | 3.3391 | 7.0175 | 0.21736 |
| 40 | 3.4906 | 11.453 | 0.21746 |

The results show that increasing the controller gains $K_{\mathrm{p}}$ and $K_{\mathrm{d}}$ (with $K_{\mathrm{d}} = 0.01 \cdot K_{\mathrm{p}}$) generally improves tracking accuracy and reduces system delay. However, when the gains become too high—such as $K_{\mathrm{p}} = 4000$ and $K_{\mathrm{d}} = 40$—the stepper motors exhibit unstable behavior, including missed steps, transient tracking loss, and occasional overshoot. These issues arise from the limited dynamic response of the 42-series stepper motors, which cannot follow high-speed control commands effectively. These findings underscore the importance of balancing control performance with actuator capabilities. While higher gains may improve theoretical performance, they can also lead to hardware-induced degradation. Considering both accuracy and reliability, the parameter configuration $K_{\mathrm{p}} = 3000$, $K_{\mathrm{d}} = 30$, and $K_{\mathrm{i}} = 0$ is selected as optimal in this study. It delivers low *MSE* and *MaxAE* while maintaining stable and smooth operation without actuator saturation. All tested configurations maintain system stability with no observed divergence.

### *5.2. Platform Attitude Tracking Performance*

In this experiment, manual disturbances were applied to the attitude sensor to simulate roll and pitch attitude variations of the platform. The compensation system actively drove

the platform's recovery window in real time, enabling it to track the target angles output by the attitude sensor and thus achieve active compensation of the window's spatial attitude. Representative experimental results are shown in Figure 16, where (a) depicts the roll angle tracking curves and (b) illustrates the tracking curves of the window midpoint height in the pitch direction. The results demonstrate that the platform window was able to follow the target attitude variations closely, achieving real-time compensation for attitude disturbances.

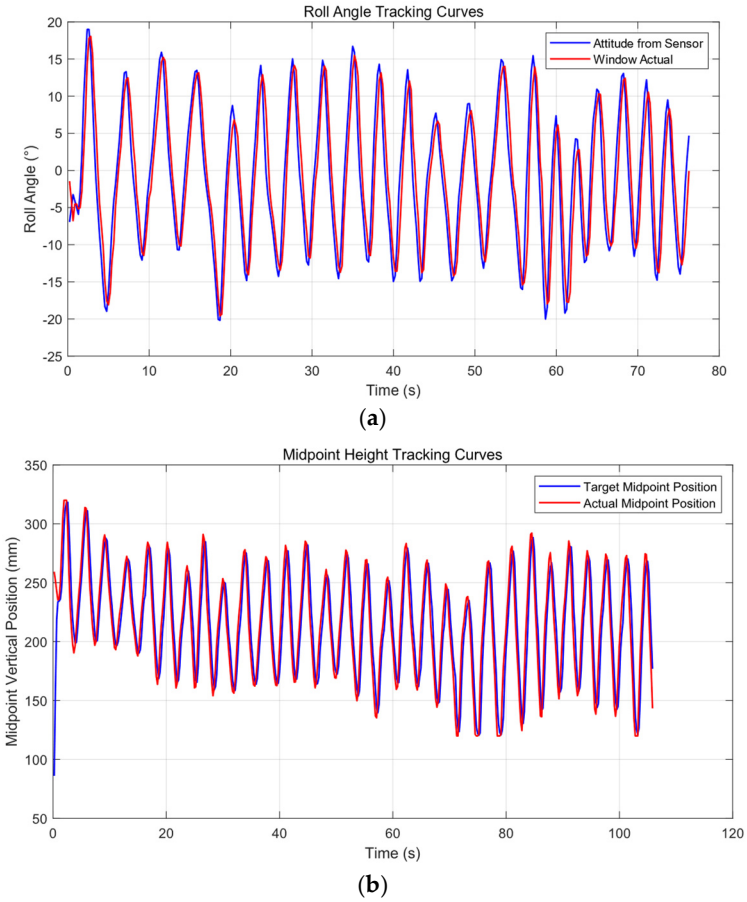



**Figure 16.** Attitude tracking results of the platform window: (**a**) roll angle tracking curves; (**b**) midpoint height tracking curves in pitch direction.

In the roll experiments, the system exhibited an average delay of 0.223 s. Without compensation, the $MSE$ of the window angle was 9.26°, and the $MaxAE$ was 20.18°. After compensation was enabled, the $MSE$ decreased to 4.13°, and the MaxAE was reduced to 11.41°, indicating that the compensation mechanism significantly improved the tracking accuracy and stability of the window angle relative to the attitude target.

In the pitch experiments, the system delay was 0.217 s. Without compensation, the $MSE$ of the window midpoint height was 82.60 mm, and the $MaxAE$ was 164.40 mm. With compensation, the $MSE$ was reduced to 19.48 mm and the $MaxAE$ to 43.50 mm, demonstrating a substantial enhancement in tracking performance.

These results indicate that the proposed compensation mechanism significantly improves tracking performance compared to the uncompensated baseline. Specifically, in the roll experiments, the $MSE$ and $MaxAE$ were reduced by 55.4% and 43.5%, respectively. In the pitch experiments, the $MSE$ and $MaxAE$ were reduced by 76.4% and 73.5%, respectively. These reductions clearly demonstrate the effectiveness of the compensation system in enhancing spatial alignment and stability under dynamic disturbances.

These results confirm that the proposed compensation mechanism enables real-time active adjustment of the window attitude and provides effective suppression of roll and pitch disturbances. The significant reduction in both $MSE$ and $MaxAE$ indicates strong tracking accuracy and disturbance rejection capability.

Moreover, the system remained stable across all tested gain configurations and disturbance inputs. No divergence or oscillatory behavior was observed, confirming the effectiveness and robustness of the implemented control strategy under real-time conditions.

Compared with conventional recovery systems that either adopt passive tensioning or rely on complex multi-DOF platforms [9,14], the proposed solution offers a lightweight and low-cost mechanical design, while still achieving robust dynamic compensation. Furthermore, unlike prior works that remain at the simulation stage [16–18], this study provides a validated physical prototype with experimental evidence, demonstrating superior practicality and engineering feasibility under representative sea conditions.

### *5.3. Extreme Disturbance Experiments and System Limitations*

Under extreme conditions involving abrupt disturbances or large, rapid changes, the attitude tracking performance of the system window declines significantly. As shown in Figure 17, the system exhibits response delays and substantial short-term increases in tracking error. Experimental results indicate that, without compensation, the platform window achieves a $MSE$ of 47.08° and a maximum absolute error of 103.67°. After enabling the compensation system, the $MaxAE$ is 46.21° and the maximum absolute error is 103.05°, with only marginal improvement. This suggests that the current system has limited compensation capability under high-intensity extreme disturbances.

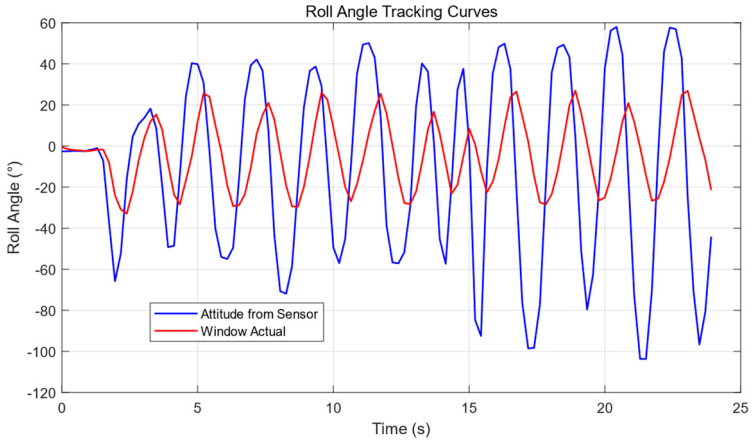



**Figure 17.** Roll angle tracking performance of the platform under extreme disturbance conditions.

The analysis suggests that this limitation is primarily due to the dynamic performance of the stepper motors and the inherent inertia of the mechanical structure, resulting in insufficient system response bandwidth and an inability to quickly follow high-frequency or extreme disturbances. To further enhance the dynamic response of the compensation system under complex operating conditions, future improvements may include adopting high-performance servo motors, optimizing the mechanical structure, and increasing the response speed and robustness of the control algorithms.

### *5.4. Dual-Channel Coordinated Compensation Experiments*

To further verify the overall compensation performance of the system under dual-channel coordinated control, both the roll angle and the window midpoint vertical position were selected as target variables for the joint compensation experiments. During the tests, the platform was subjected to simultaneous roll and pitch disturbances, while the

compensation system performed real-time closed-loop control to actively regulate both the window's spatial orientation and vertical position.

The experimental results are shown in Figure 18, which presents the time-domain tracking curves of the window roll angle and midpoint height under dual-channel coordinated compensation. As can be seen, the actual trajectories closely follow the target references in both channels, demonstrating effective real-time compensation of the window's attitude and spatial position.

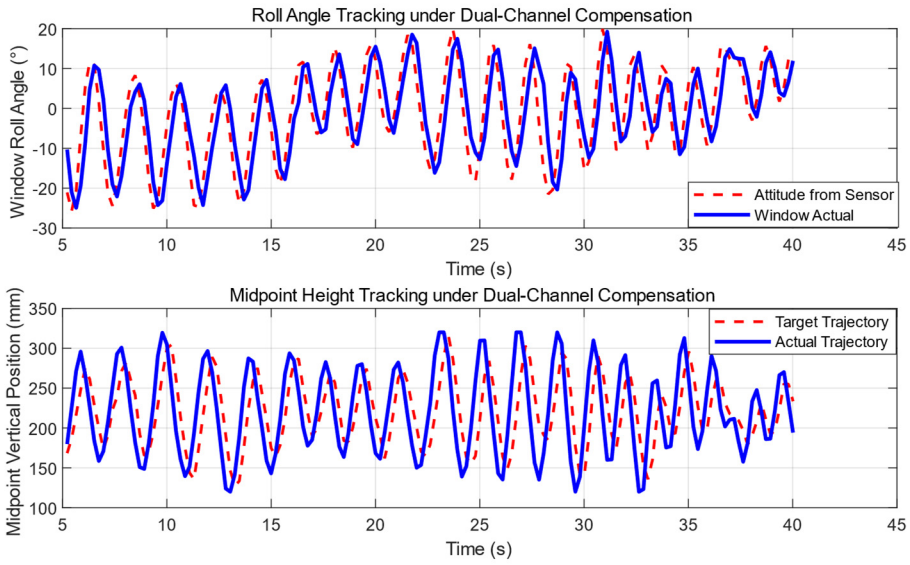



**Figure 18.** Time-domain tracking curves of the window roll angle and midpoint height under dual-channel coordinated compensation.

Quantitative evaluation shows that, for the roll channel, the compensated $MSE$ is 7.36°, and the $MaxAE$ is 21.64°. For the midpoint height channel, the compensated $MSE$ is 47.11 mm, and the $MaxAE$ is 106.30 mm. Compared with the uncompensated case, the tracking errors in both channels are significantly reduced. Moreover, peak-based delay analysis indicates an average response delay of 0.223 s for the roll channel and 0.217 s for the midpoint height channel, verifying the system's rapid dynamic response capability.

These results confirm that the proposed multi-channel coordinated compensation strategy can effectively enhance the spatial attitude stability and position tracking accuracy of the platform under complex multi-degree-of-freedom disturbances, demonstrating good engineering feasibility and application potential.

## 6. Conclusions

This study focused on the attitude compensation requirements of a ramp-based AUV recovery system and developed a desktop-scale physical experimental platform integrating attitude acquisition based on an attitude sensor, a dual-motor-driven compensation mechanism, and a closed-loop control system. Through a series of disturbance experiments, it was verified that the proposed compensation mechanism can effectively achieve dynamic tracking and real-time compensation of the platform window in both roll and pitch directions. The experimental results demonstrate that the system exhibits excellent attitude tracking accuracy and response speed, and that the dual-channel compensation ensures high stability. This provides strong support for the stability of the AUV recovery window and the success rate of docking operations. The PID-based center-tracking compensation strategy for pitch also lays an engineering foundation for the extension of the system to multi-degree-of-freedom applications. The comparative analysis of control parameters and

repeated experiments further validates the engineering feasibility and practical value of the platform.

Despite the demonstrated effectiveness of the compensation system, several limitations remain. First, the use of open-loop stepper motors limits the dynamic response, especially under high-gain or high-frequency excitation, leading to occasional missed steps or tracking delays. Second, the disturbance signals in this study were manually generated and may not fully reflect the stochastic nature and spectral content of real sea waves. Third, the experiments were conducted only on a desktop platform, which lacks hydrodynamic coupling and does not replicate actual marine deployment scenarios. Fourth, the current compensation strategy only considers the recovery platform's angular motion and does not account for the linear motion components, particularly heave, which also affect the capture window's vertical position. Finally, the system does not model dynamic interactions with the AUV body or mutual motion coupling during docking.

To address these issues, future efforts will focus on replacing the stepper motors with servo actuators to enhance the system's response bandwidth and disturbance rejection capabilities. The disturbance model will be upgraded to include stochastic wave profiles or programmable wave tank tests for more realistic simulation. Additionally, onboard validation will be carried out using a full-scale prototype installed on a USV. Coupled motion modeling and control between the recovery platform and AUV will also be introduced to improve overall system robustness and coordination. Furthermore, heave sensing and vertical compensation will be incorporated to extend the current two-axis mechanism to full spatial disturbance handling, thereby improving docking success under complex sea conditions.

**Author Contributions:** Conceptualization, Z.Q. and L.M.; Methodology, Z.Q.; Software, Z.Q. and J.W.; Validation, Z.Q. and Z.G.; Investigation, C.L.; Resources, H.G.; Data curation, Z.G.; Writing—original draft preparation, Z.Q.; Writing—review and editing, L.M.; Visualization, Z.Q. and Z.G.; Supervision, L.M.; Project administration, H.G.; Funding acquisition, L.M. All authors have read and agreed to the published version of the manuscript.

**Funding:** This work was supported by the National Natural Science Foundation of China (Grant No. 52301391) and the Basic Research Program of the Chinese Academy of Sciences (Grant No. 2023JCG0) and the National Projects of China (Grant Nos. WDZC2025290306 and WDZC2025290303).

**Data Availability Statement:** The data presented in this study are available on request from the corresponding author.

**Conflicts of Interest:** The authors declare no conflicts of interest.

## References

1. Xu, Y.L.; Du, J.H.; Lei, Z.Y.; Cai, Y.Y.; Ye, Z.Y.; Han, Z.Y. Applications Status and Key Technologies of Underwater Robots in Fishery. *Robot* **2023**, *45*, 110–128.
2. Kang, S.; Yu, J.C.; Zhang, J. Research Status of Micro Autonomous Underwater Vehicle. *Robot* **2023**, *45*, 218–237.
3. Meng, L.S.; Li, M.S.; Ling, Y.; Wang, Z.C. Launch and Recovery Technology of Autonomous Underwater Vehicle. *Unmanned Syst. Technol.* **2023**, *7*, 1–19.
4. Ponzini, F.; Fruzzetti, C.; Sabatino, N. Real-time critical marine infrastructure multi-sensor surveillance via a constrained stochastic coverage algorithm. In Proceedings of the iSCSS, 2024, Liverpool, UK, 5–7 November 2024.
5. Bitar, G.; Martinsen, A.B.; Lekkas, A.M.; Breivik, M. Trajectory planning and control for automatic docking of ASVs with full-scale experiments. *IEEE J. Ocean Eng.* **2020**, *45*, 128–140. [CrossRef]
6. Xu, H.; Shangguan, X.-C.; Li, J.; Chen, W.-H. Recovery control of autonomous underwater vehicles based on modified delay-product-type functional. *Appl. Math. Model.* **2025**, *137*, 115713. [CrossRef]
7. Sarda, E.I.; Dhanak, M.R. Launch and recovery of an autonomous underwater vehicle from a station-keeping unmanned surface vehicle. *IEEE J. Ocean Eng.* **2018**, *44*, 290–299. [CrossRef]

8. Song, T.; Zheng, R.; Liang, H.G. Design and Research of Autonomous Launch and Recovery Device for Underwater Towed Vehicle. *Ship Sci. Technol.* **2020**, *42*, 96–101.
9. Zhang, M.Y.; Meng, L.S.; Li, M.S.; Gu, H.T.; Wang, Z.W. Design and implementation of an inclined sliding rail autonomous recovery AUV device. *Ship Sci. Technol.* **2025**, *47*, 50–55.
10. Liu, J.; Yu, F.; He, B.; Soares, C.G. A review of underwater docking and charging technology for autonomous vehicles. *Ocean Eng.* **2024**, *297*, 117154. [CrossRef]
11. Fan, S.; Liu, C.; Li, B.; Xu, Y.; Xu, W. AUV Docking Based on USBL Navigation and Vision Guidance. *J. Mar. Sci. Technol.* **2019**, *24*, 673–685. [CrossRef]
12. Stokey, R.; Allen, B.; Austin, T.; Goldsborough, R.; Forrester, N.; Purcell, M.; von Alt, C. Enabling technologies for REMUS docking: An integral component of an autonomous ocean-sampling network. *IEEE J. Ocean Eng.* **2001**, *26*, 487–497. [CrossRef]
13. Chu, S.; Lin, M.; Li, D.; Lin, R.; Xiao, S. Adaptive reward shaping based reinforcement learning for docking control of autonomous underwater vehicles. *Ocean Eng.* **2024**, *318*, 120139. [CrossRef]
14. Gutnik, Y.; Zagdanski, N.; Farber, S.; Treibitz, T. Navigating ALICE: Advancements in deployable docking and precision detection for AUV operations. *Robotics* **2024**, *14*, 5. [CrossRef]
15. Li, X.; Zhang, H.; Li, S.; Sun, X. Dynamic modeling and motion compensation of an AUV recovery device based on sliding rail structure. *Ocean Eng.* **2023**, *274*, 113888.
16. Batista, P.; Silvestre, C.; Oliveira, P. A two-step control approach for docking of autonomous underwater vehicles. *Int. J. Robust Nonlinear Control* **2015**, *25*, 1528–1547. [CrossRef]
17. Palomeras, N.; Ridao, P. Autonomous Underwater Vehicle Docking Under Realistic Assumptions Using Deep Reinforcement Learning. *Drones* **2024**, *8*, 673. [CrossRef]
18. Jin, T.; Yang, X.; Qi, C.; Wu, Y.; Li, Z.; Chen, H. Model reference adaptive PID control for enhanced stability and posture control of unmanned underwater vehicles. *Ocean. Eng.* **2025**, *330*, 121218. [CrossRef]
19. Bingül, Z.; Gul, K.M. Intelligent-PID with PD feedforward trajectory tracking control of an autonomous underwater vehicle. *Machines* **2023**, *11*, 300. [CrossRef]
20. Sharkawy, A.N.; Koustoumpardis, P. Dynamics and Computed-Torque Control of a 2-DOF manipulator: Mathematical Analysis. *Int. J. Adv. Sci. Technol.* **2019**, *28*, 201–212.
21. Teo, K. A Robust Fuzzy Autonomous Underwater Vehicle (AUV) Docking Approach for Unknown Current Disturbances. *IEEE J. Ocean Eng.* **2012**, *37*, 347–357. [CrossRef]
22. Xiong, Y.; Pan, L.; Xiao, M.; Xiao, H. Motion control and path optimization of intelligent AUV using fuzzy adaptive PID and improved genetic algorithm. *Math. Biosci. Eng.* **2023**, *20*, 9208–9245. [CrossRef] [PubMed]
23. Lin, R.; Zhao, Y.; Li, D.; Lin, M.; Yang, C. Underwater Electromagnetic Guidance Based on the Magnetic Dipole Model Applied in AUV Terminal Docking. *J. Mar. Sci. Eng.* **2022**, *10*, 995. [CrossRef]
24. Zhang, T.; Li, D.; Yang, C. Study on impact process of AUV underwater docking with a cone-shaped dock. *Ocean Eng.* **2017**, *130*, 176–187. [CrossRef]
25. Jørgensen, E.K.; Fossen, T.I.; Bryne, T.H.; Schjølberg, I. Underwater position and attitude estimation using acoustic, inertial, and depth measurements. *IEEE J. Ocean Eng.* **2020**, *45*, 64–79. [CrossRef]
26. Lin, M.; Lin, R.; Yang, C.; Li, D.; Zhang, Z.; Zhao, Y.; Ding, W. Docking to an underwater suspended charging station: Systematic design and experimental tests. *Ocean Eng.* **2022**, *249*, 110766. [CrossRef]
27. Kim, A.; Eustice, R.M. Real-Time Visual SLAM for Autonomous Underwater Hull Inspection Using Visual Saliency. *IEEE Trans. Robot.* **2013**, *29*, 719–733. [CrossRef]
28. Krauss, S.T.; Stilwell, D.J. Unscented Kalman Filtering on Manifolds for AUV Navigation—Experimental Results. *arXiv* **2022**, arXiv:2210.06510.
29. Astrom, K.J.; Murray, R.M. *Feedback Systems: An Introduction for Scientists and Engineers*; Princeton University Press: New York, NY, USA, 2008.
30. Carlsson, S.; Åström, K. Multi-Sensor Fusion for Underwater Vehicle Localization: Comparisons of MSE and MaxE in attitude estimation. *Sensors* **2021**, *21*, 1149.
31. Knapp, C.H.; Carter, G.C. The generalized correlation method for estimation of time delay. *IEEE Trans. Acoust Speech Signal Process.* **1976**, *24*, 320–327. [CrossRef]
32. Benesty, J.; Chen, J.; Huang, Y. Time-delay estimation via linear interpolation and cross-correlation. *IEEE Trans. Speech Audio Process.* **2004**, *12*, 509–518. [CrossRef]
33. Seborg, D.E.; Edgar, T.F.; Mellichamp, D.A. *Process Dynamics and Control*, 2nd ed.; Wiley: Hoboken, NJ, USA, 2004.


**Disclaimer/Publisher's Note:** The statements, opinions and data contained in all publications are solely those of the individual author(s) and contributor(s) and not of MDPI and/or the editor(s). MDPI and/or the editor(s) disclaim responsibility for any injury to people or property resulting from any ideas, methods, instructions or products referred to in the content.